Tailoring Lithiation Behavior by Interface and Bandgap Engineering at the Nanoscale

Yang Liu,*[†,⊥] Xiao Hua Liu,[†,⊥] Binh-Minh Nguyen,[‡,§] Jinkyoung Yoo,[‡] John P. Sullivan,[∥] S. Tom Picraux,[‡] Jian Yu Huang,[†] and Shadi A. Dayeh*[‡,§]

[†]Center for Integrated Nanotechnologies, Sandia National Laboratories, Albuquerque, New Mexico 87185, United States
[‡]Center for Integrated Nanotechnologies, Los Alamos National Laboratory, Los Alamos, New Mexico 87545, United States
[§]Department of Electrical and Computer Engineering, University of California San Diego, La Jolla, California 92093, United States
[∥]Materials Physics Department, Sandia National Laboratories, Livermore, California 94551, United States

S *Supporting Information*

ABSTRACT: Controlling the transport of lithium (Li) ions and their reaction with electrodes is central in the design of Li-ion batteries for achieving high capacity, high rate, and long lifetime. The flexibility in composition and structure enabled by tailoring electrodes at the nanoscale could drastically change the ionic transport and help meet new levels of Li-ion battery performance. Here, we demonstrate that radial heterostructuring can completely suppress the commonly observed surface insertion of Li ions in all reported nanoscale systems to date and to exclusively induce axial lithiation along the ⟨111⟩ direction in a layer-by-layer fashion. The new lithiation behavior is achieved through the deposition of a conformal, epitaxial, and ultrathin silicon (Si) shell on germanium (Ge) nanowires, which creates an effective chemical potential barrier for Li ion diffusion through and reaction at the nanowire surface, allowing only axial lithiation and volume expansion. These results demonstrate for the first time that interface and bandgap engineering of electrochemical reactions can be utilized to control the nanoscale ionic transport/insertion paths and thus may be a new tool to define the electrochemical reactions in Li-ion batteries.

KEYWORDS: *Interface effect, bandgap engineering, lithiation behavior, Ge/Si core/shell nanowire, in situ TEM study*
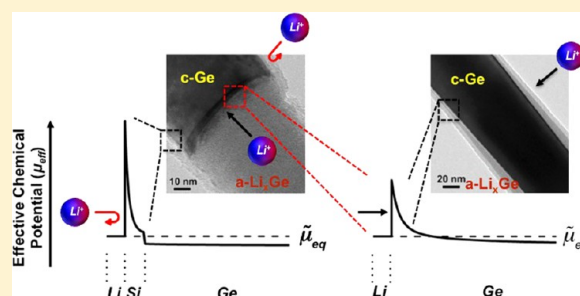
Lithium-ion batteries are the backbone power devices for a wide variety of existing and emerging applications including portable electronics, electric vehicles, and stationary power backup for fluctuating energy sources. These applications are demanding radical improvement of lithium-ion batteries to have higher energy and power densities, good cyclability, and low cost.[1,2] To meet the ever-increasing demand of higher battery performance, new materials and novel device structures are being aggressively pursued. For instance, compared to the carbonaceous anode used in today's lithium-ion batteries, silicon (Si) and germanium (Ge) are being widely studied as new anode materials that could potentially boost electrode energy density by up to ten times. However, huge volume changes during the lithium (Li) insertion and extraction cycles are intrinsically associated with the desired high storage capacity, causing rapid degradation of the electrodes.[3−6] Nanostructured and nanocomposite materials, such as nanoparticles, nanotubes, and nanowires, are being explored extensively as the building blocks of next generation electrodes because they offer facile strain relaxation, fast electron and ion transport paths at the nanoscale, and large surface areas for functionalization.[7−12]

Parallel to the efforts of seeking for new materials and device architectures, understanding of the underlying reaction mechanisms is crucially important for the rational design of high performance Li-ion batteries. The electrochemical reactions in an electrode material, denoted as M, involve lithiation that is defined as the alloying reaction between Li and M to form a lithiated phase, Li_xM, or the reverse process of delithiation. The lithiation behavior of M is usually found to be intrinsic to the specific material itself, such as preferential insertion routes along certain crystallographic directions, and is less sensitive to the test conditions.[13,14] For example, the lithiation of single-crystal Si has been found to be highly anisotropic in both the in situ and ex situ experiments[15−17] with the largest volume expansion along ⟨110⟩ directions and the minimum along ⟨111⟩ directions.[18,19] However, despite having the same diamond cubic crystal structure as Si, Ge shows nearly isotropic lithiation,[14,20] and lithiation onset voltages are not dependent on crystal orientations.[21] In general, it is highly desirable to define the Li insertion routes and the
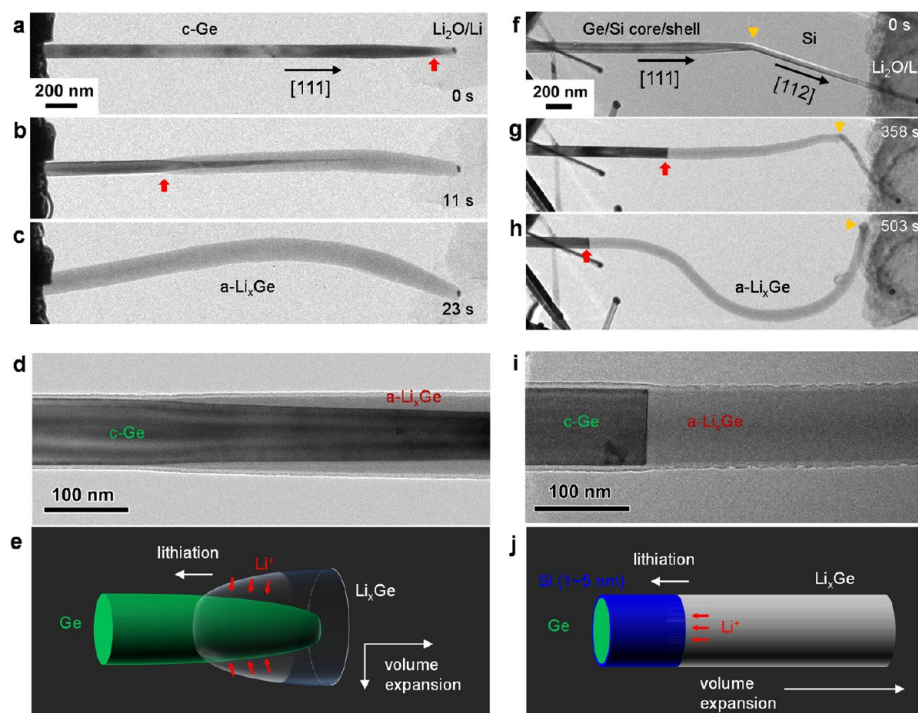
Figure 1. Core−shell versus axial lithiation of Ge nanowires with and without an ultrathin Si shell. (a−c) TEM image series showing the core−shell lithiation of a pure Ge nanowire without any shell layer. The pristine crystalline Ge (c-Ge) nanowire was grown along the [111] direction. During lithiation front propagation (marked by the red arrows), Li insertion from the nanowire surfaces gradually converted the c-Ge with a dark contrast into amorphous Li_xGe (a-Li_xGe) alloy with a gray contrast. The intermediate structure had a tapered c-Ge core wrapped by the a-Li_xGe shell. The fully lithiated wire was both wider and somewhat longer than the original c-Ge wire, indicating both radial and axial volume expansion during lithiation. (d) Close view of the reaction front area in pure Ge nanowire, showing the tapered shape phase boundary. (e) Schematic illustration of the core−shell lithiation in pure Ge nanowires. (f−h) TEM image series showing the axial lithiation behavior of a Ge/Si core/shell nanowire with a thinner extended Si segment atop that grew epitaxially at a 19.5° tilt in growth direction from [111] to [112]. Lithiation of the Ge/Si core/shell segment was completely axial, with a moving phase boundary roughly parallel to the nanowire cross section that converted c-Ge into a-Li_xGe. The lithiated wire elongated significantly but showed little radial swelling. (i) Close view of the reaction front area in Ge/Si core/shell nanowire, showing the axial lithiation behavior in sharp contrast with the image in (d). (j) Schematic illustration of the axial lithiation induced by an ultrathin Si shell layer on Ge nanowires. With the 1 nm thick Si layer, the Li transport path and insertion are drastically changed as well as the volume expansion.

accompanying volume changes, which have large impacts on the mechanical deformation, durability, and kinetics of the electrodes. One of the straightforward ways to control the lithiation and deformation is to apply an external mechanical confinement. For instance, the radial expansion of a SnO_2 nanowire can be completely suppressed by carbon, copper, or aluminum coatings,[22] and an outer SiO_2 layer can also force the inner Si tube to expand inward to the hollow cavity upon lithiation.[9] However, such mechanical confinements usually require a coating layer that is thick and rigid, which can be sensitive to manufacturing defects, and may reduce the overall specific cell capacity due to the added weight.[23]

Batteries, as electronic devices, require both mass and charge transport in a harmonious manner during their operation. The flow of charges has huge impacts on the materials. For instance, the direction of volume expansion is perpendicular to the lithiation reaction front (i.e., the interface between Li_xM and M), as if the Li ions are digging into the anode material and pushing the lithiated products in their wake. Therefore, the volume expansion could be also controlled by defining the Li insertion direction. As the electrons and Li ions must meet to initiate lithiation, this requires manipulation of the charged particles (electrons, Li ions, or both) to flow in a controlled manner. In the past two decades, it has been shown that ionic transport properties can be dominated by interfaces at the nanoscale,[24−28] which provides the possibility to control the Li

diffusion pathways and to modify the volume expansion direction by introducing heterojunctions (namely chemical and structural discontinuities). Moreover, if the materials across the junction interface are properly chosen the energy band-edge of the heterostructure can be further controlled to tailor the properties of the material. Such bandgap engineering is key to tailoring the performance of electronic devices, such as high-mobility field effect transistors,[29−31] laser diodes,[32] high-performance thermoelectric materials,[33] and high-efficiency water-splitting devices.[34] Similarly, potential barriers can be introduced into the Li-ion battery electrode materials via bandgap engineering, which can hinder the Li ions or electrons transport in certain directions while promoting transport in other directions. Therefore, as an electrochemical device, it is anticipated that the lithiation behavior of a battery electrode may also be controlled by band structure engineering through creation of suitable interfaces to modulate the movement of charged particles.

The in situ transmission electron microscopy (TEM) electrochemistry technique has become a powerful approach to understand lithiation behaviors and reaction chemistries during battery operation due to the unique capability of dynamically resolving the structural evolution, phase transformation, and chemical composition change of electrodes with high resolution.[13,14] Various Li-ion battery materials have been studied, including Si with different geometry such as nano-
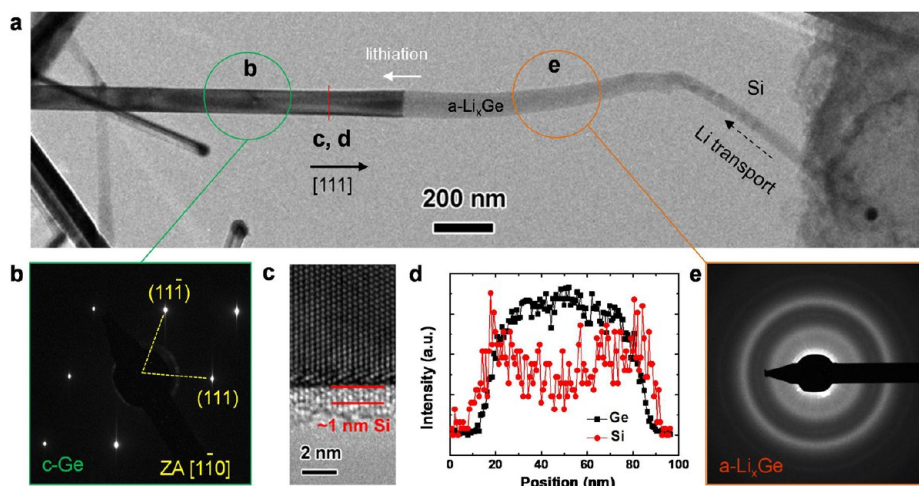
Figure 2. Microstructure of the Ge/Si nanowire during the axial lithiation. (a) An overview of a Ge/Si core/shell nanowire during lithiation. The axial lithiation was ongoing in the Ge segment, but the Si segment remained almost intact without appreciable volume expansion, suggesting that Li transport must have taken place by surface diffusion on the Si segment. This also proves that Li insertion into Ge is much easier than into Si. (b) Electron diffraction pattern of the unreacted Ge/Si core/shell nanowire exhibiting single crystal. (c) High-resolution TEM image showing the epitaxial Si shell of 1 nm thick on the c-Ge core. (d) STEM-EDX line scan showing the Ge K_α and Si K_α intensity profiles across the Si-coated Ge nanowire (red line in panel a) and confirming the Ge/Si core/shell structure. (e) Electron diffraction pattern of a-Li$_x$Ge alloy after lithiation.

wires,[15,19,35] nanorods,[36] nanoparticles,[37] and nanobeads,[38] integrated Si with other materials such as Si nanoparticles in a carbon matrix,[39] metallic coatings on Si nanowires,[40] and amorphous Si on carbon,[41] Ge nanowires,[20] and conversion-type materials such as CuO nanowires[42] and FeF$_2$ nano-particles,[43] which greatly advanced understanding of the kinetics, reaction mechanisms, and mechanical responses in these complex systems. Therefore, the in situ TEM electro-chemistry offers a feasible and reliable method to investigate the lithiation behaviors in the heterostructures and the effects of interface and bandgap engineering on the structures, especially at the nanoscale.

In this report, we demonstrate for the first time that the lithiation behavior of a Ge nanowire can be dramatically changed by interface and bandgap engineering, that is, by applying an epitaxial ultrathin Si shell layer. Individual pure Ge nanowires and those with different shells on their surfaces were lithiated inside a TEM; the details of materials synthesis, surface treatments, and in situ electrochemical experiments can be found in the Supporting Information.

Thin Si Coating Drastically Changes the Lithiation of Ge Nanowires. Figure 1 contrasts the dramatically different lithiation behaviors of individual crystalline Ge (c-Ge) nanowires without and with a thin Si shell layer. The Ge nanowires were epitaxially grown on a Ge(111) wafer, with a growth direction along [111] that is perpendicular to the substrate surface. Figure 1a−c and Movie S1 in Supporting Information show the structural evolution of such a pure Ge nanowire upon lithiation. The reaction front (marked by red arrow heads) propagated progressively along the nanowire. The Li ions diffused along the surface and were simultaneously inserted into the Ge nanowire from the radial directions, resulting in a lithiated Li$_x$Ge shell on a tapered, unreacted crystalline Ge core (Figure 1b). The lithiated nanowire (Figure 1c) swelled along both axial and radial directions, indicating the lithiation of [111]-oriented Ge nanowires is also approximately isotropic, consistent with the lithiation of [112]-oriented Ge nanowires.[20] After lithiation, the nanowire was transformed to an amorphous Li$_x$Ge (a-Li$_x$Ge) alloy with a gray contrast

(Figure 1c).[20] The phase boundary between c-Ge and a-Li$_x$Ge forms a long, conical interface (Figure 1b), as clearly shown in the close view (Figure 1d), so the Li insertion is mainly along the radial directions in an uncoated Ge nanowire, as manifested by significant swelling plus some elongation after full lithiation (Figure 1c). Figure 1e is a schematic drawing highlighting the reaction front of a tapered c-Ge core and swelling a-Li$_x$Ge shell.

An ultrathin Si shell layer with controlled thickness between 1 and 5 nm was grown on the [111] Ge nanowires by switching the Ge-containing precursor (30% GeH$_4$ in H$_2$) to the Si-containing precursor (50% SiH$_4$ in H$_2$) in the nanowire synthesis, which results in a thin epitaxial Si shell over the Ge nanowire and also a thin Si nanowire extension at the Ge tip (see the Supporting Information for further details).[44] The Si segment grew along the [112] direction, thus formed a 19.5° kink with respect to the [111] Ge wire (Figure 1f).[44] The thin Si shell layer on the [111] Ge nanowire drastically changed the lithiation behavior, as shown in Figure 1f−i (and Supporting Information Movie S2). The radial lithiation and swelling were completely suppressed, as if the Li ion transport and insertion could only occur along the axial direction. The reaction front was transformed to the cross section of the nanowire, as marked by the red arrows, which was verified by the close view image in Figure 1i. Given the thinness of the Si shell layer, it is quite intriguing to see such a drastic change, as schematically illustrated in Figure 1e versus Figure 1j.

The electron beam effect is an important issue to consider when conducting the in situ TEM experiments. Lithiation experiments with different electron dosage rates, including beam off condition, were carried out on the Ge/Si core/shell nanowires (Supporting Information Figures S1−S2), which clearly show that the axial lithiation manner was not altered in a wide range of electron beam intensity. However, electron beam irradiation does show some perceivable effects in a lithiated nanowire that is imaged at high magnifications when the lithiation voltage is not present. The diameter of a lithiated segment became slightly smaller than that immediately after lithiation (Figure 1i) due to the electron beam induced delithiation (see Figure S3 in the Supporting Information for
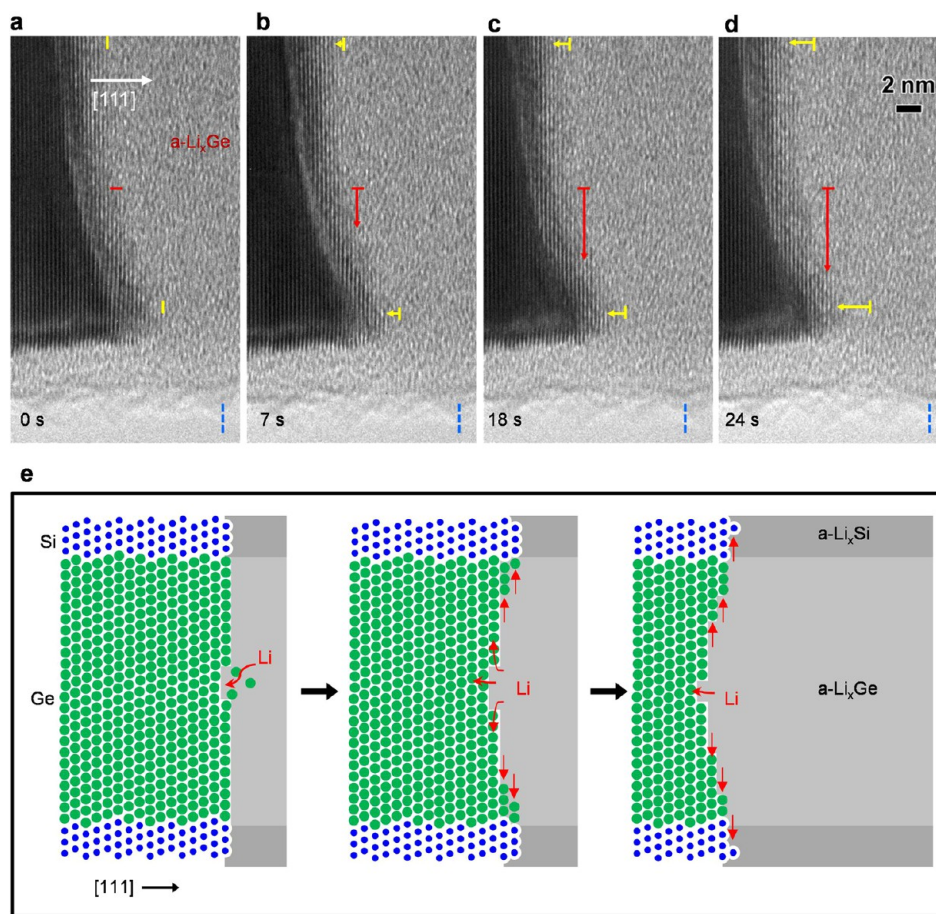
Figure 3. Ledge mechanism revealed by high-resolution imaging of the axial lithiation in a Ge/Si core/shell nanowire. (a−d) TEM image series showing evolution of the Ge crystal close to the surface during the axial lithiation. As revealed with high resolution, the local phase boundary shows a concave shape and lithiation occurred from the nanowire center outward to the surface through a ledge mechanism. The yellow arrows mark the progress of macroscopic lithiation, which is parallel to the nanowire axis of [111]; the red arrows mark the microscopic mechanism of ledge flow, which is perpendicular to [111]; the blue dash lines mark a surface feature as reference. The contrast at the interface indicates a bowl-like shape of the phase boundary with possible radial lithiation from nanowire center to the circumference. (e) Schematic illustration of the ledge mechanism. The macroscopic lithiation is along the axial direction of [111], while the microscopic lithiation is taking place by depletion of the {111} planes along the ⟨110⟩ or ⟨112⟩ directions via ledge flow. The curved phase boundary is a clear indicative of suppression of Li insertion from the surface.

more details). Nonetheless, given the consistency of the reproducible lithiation behavior with different dosage rates, the beam effect on the lithiation behavior (axial versus core/shell) can be safely excluded.

In order to further exclude the influence from the top Si segment on the axial lithiation behavior in the Ge/Si core/shell nanowire, the following two control experiments were performed: (1) the top Si segment was mechanically removed (by knocking-off) and the remaining Ge base was lithiated (Supporting Information Figure S4); and (2) the Si−Ge sequence was connected in reverse into the same TEM holder lithiation setup to change the polarity of the built-in electric field (Supporting Information Figure S5). In both cases, the axial lithiation of the Si-coated Ge segments was observed without perceivable difference. This indicates that the extra Si segment on the top has little effects on the lithiation of the Si-coated Ge nanowire base. Strikingly, the Si shell epitaxially grown on the Ge nanowire surfaces, despite of its thinness, seems to play a decisive role in defining the lithiation behavior of the relatively bulky Ge nanowire.

Figure 2 shows the microstructure of the Ge/Si core/shell nanowire during the axial lithiation. In the low magnification image (Figure 2a), a flat interface separates the unreacted c-Ge

on the left and a-Li$_x$Ge on the right with apparent contrast difference. The Si segment in contact with the Li$_2$O/Li electrode shows a crystalline contrast but no swelling, indicating that it remained almost intact although lithiation had been occurring beyond in the Ge segment that was farther from the Li source. This observation suggests that Li transport must have taken place by surface diffusion on the Si segment, and more importantly, it proves that Li insertion into Si is much more difficult than into Ge. Figure 2b shows the electron diffraction pattern (EDP) from the unreacted Ge/Si core/shell nanowire segment, in which only c-Ge single crystal pattern is revealed. However, the surface Si layer of about 1 nm thick was confirmed by the high-resolution TEM (HRTEM) image (Figure 2c) and scanning TEM (STEM) energy-dispersive X-ray spectroscopy (EDX) line scan (Figure 2d). The lithiated phase shows two broad diffuse halos in the EDP (Figure 2e), indicating formation of the a-Li$_x$Ge alloy.[20] The microstructural characterization of the phase transformations essentially suggests similar amorphization process upon Li insertion into the c-Ge lattice in both cases.

Ledge Mechanism: Layer-by-Layer Lithiation from Nanowire Center toward Surfaces. Our in situ TEM study has shown that Li insertion into Si crystals along ⟨111⟩ is

extremely difficult, which is the root cause of the anisotropic lithiation in crystalline Si.[19] Therefore, it is surprising to see that Li insertion into a Ge crystal can take place almost exclusively along ⟨111⟩. With the capability of real-time high-resolution microscopy, we carried out the atomic-scale imaging of the lithiation process of the Ge/Si core/shell (1 nm thick shell) nanowire, focusing on the evolution of the regions close to the surface (Figure 3a−d). In Figure 3a, the yellow lines mark two visible (111) planes at the amorphous−crystalline interface (ACI), with one close to the nanowire surface and the other close to the center. The two (111) planes were initially separate by a few nanometers from each other, because the ACI was curved. As one can see that the ACI was not flat, there are always lattice fringes overlapping the a-Li$_x$Ge. This is because the surface region was always lithiated at a later time than the center, thus the ACI has a concave shape and forms this superimposed contrast. During lithiation, the two (111) planes became invisible (Figure 3b), indicating the transformation from c-Ge to a-Li$_x$Ge. It is worth noting that the lithiation rates near the surface and near the center were almost the same, which could be varied by one or two atomic planes and represented by the length of the yellow arrows in each image (Figure 3b−d). The process of resolving (111) planes one by one illustrates the same axial lithiation rates at each point of the ACI, giving a macroscopically steady lithiation along the [111] direction. In Figure 3a, the red line marks the edge of one (111) plane, which is taken as the reference. This (111) plane was dissolved from the center toward the surface during lithiation, as indicated by the red arrows in Figure 3b−d. The atomic-scale lithiation process reveals that lithiation actually occurs through a lateral ledge flow as schematically illustrated in Figure 3e, quite similar to the key feature resolved in Si lithiation.[19] Although the apparent lithiation direction is along [111], the microscopic mechanism is still by ledge flow perpendicular to the [111] direction. Another key implication of this observation is that the close-packed Ge (111) plane is susceptible to Li insertion, as the ledges must be nucleated at the center of the nanowire. This is consistent with the isotropic lithiation of Ge crystals. Without the capability of breaking Ge (111) close-packed planes, the ledge flow direction cannot be maintained and the curved ACI would not be observed.

The Role of the Thin Si Shell. Ionic transport and reaction rates are expected to be drastically changed at heterointerfaces.[24] A lithiation reaction presupposes Li ion diffusion to and reaction at a certain material surface. To rationalize the effects of the Si shell on Ge nanowire lithiation, we refer to the analogy of chemical potential barriers for impurity−Li ion−diffusion with that of chemical potential barriers for free charge carrier transport, as discussed extensively by Maier,[24,25] and in the case of semiconductor heterointerfaces by Tersoff.[45] According to the latter analysis at semiconductor heterointerfaces, the effective potential for ions or defects at heterointerfaces is considered by moving the ion in the material by two steps: (1) moving the impurity across the interface, and (2) ionizing the impurity and returning the electron or hole to the starting position.[45] The corresponding effective potential for a Li ion, μ_{eff} can therefore be written as

$$\mu_{eff} = H_M^0 + I_M - (E_M^c - \tilde{\mu}_M) \tag{1}$$

where M is either Si or Ge, H_M^0 is the enthalpy of formation of the neutral Li defect site in M, I_M is the ionization energy for Li ion in M, E_M^c is the conduction band edge in M, and $\tilde{\mu}_M$ is the

equilibrium electrochemical potential across the whole structure. This effective potential that the Li ion experiences as it diffuses into M depends on local quantities such as composition and strain and a nonlocal quantity, E_M^c, which is determined by the distribution of charges across the entire crystal far away.[45] The Li ion is a shallow donor impurity in both Si[46] and Ge,[47] and μ_{eff} is thus dependent on the negative of the conduction band-edge. Therefore, we simulated the equilibrium band-edge profiles across Ge, Ge/Si core/shell, and Ge/Si/C core multishell nanowire structures to infer qualitative measures of the effective chemical potential barriers that a Li ion experiences for the three different structures. For simplicity, the reference energy in an unbiased cell is taken to be the Fermi energy of a Li metal shell surrounding our Ge, Ge/Si, or Ge/Si/C structures.

Figure 4a,b shows the energy band-edge profile in Si-coated and uncoated Ge nanowires, respectively, over a distance of 20
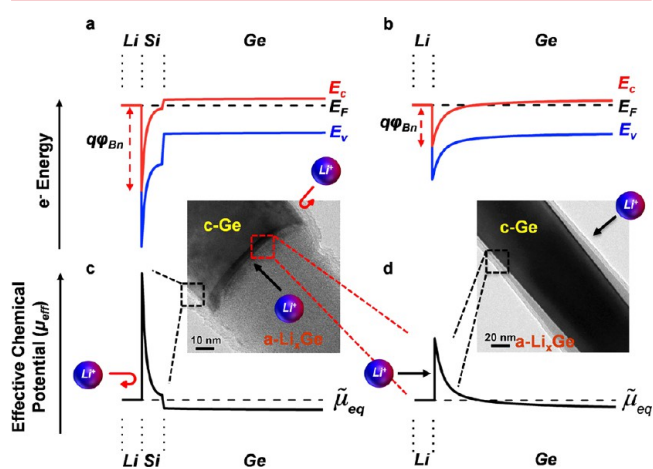
Figure 4. Comparison of band-edge profile and effective Li ion potential in Ge/Si core/shell and Ge nanowires. (a,b) Energy band-edge diagram of a Ge/Si core/shell nanowire, and a Ge nanowire, respectively, with a Li shell showing a negative Schottky barrier height that is larger for the Ge/Si core/shell than that for the Ge only nanowire. (c,d) Effective chemical potential profiles along 20 nm from the nanowire surface for Li ions in Ge/Si core/shell nanowire, and in Ge nanowire, respectively, showing a larger chemical potential barrier for the Ge/Si core/shell nanowire (c) compared to the Ge nanowire (d). Left inset is a close view of the reaction front area in Ge/Si core/shell nanowire that highlights a smaller chemical potential barrier at the planar Ge core layers compared to the Si shell at the circumference leading to axial lithiation. Right inset is a close view of the reaction front in the Ge nanowire that lacks the presence of strong chemical potential barrier at its surface and encounters therefore core−shell lithiation.

nm from the nanowire surface. Li, which has a small work function leads to a negative Schottky barrier height with Si ($q\varphi_{Bn} = -1.67$ eV) that is larger than that with Ge ($q\varphi_{Bn} = -0.8$ eV).[48] Using eq 1, the effective chemical potential for a Li ion across a Ge/Si core/shell interface and a Ge interface is shown in Figure 4c,d, respectively. A large chemical potential is experienced with the Si surface (Figure 4c) compared to a Ge surface (Figure 4d). The lower μ_{eff} for Li ion diffusion into Ge together with the fact that Li ions have higher diffusion coefficients in Ge compared to Si, especially at low temperatures,[49] explains our earlier observations that Ge nanowires[20] lithiate much faster than Si nanowires.[19]
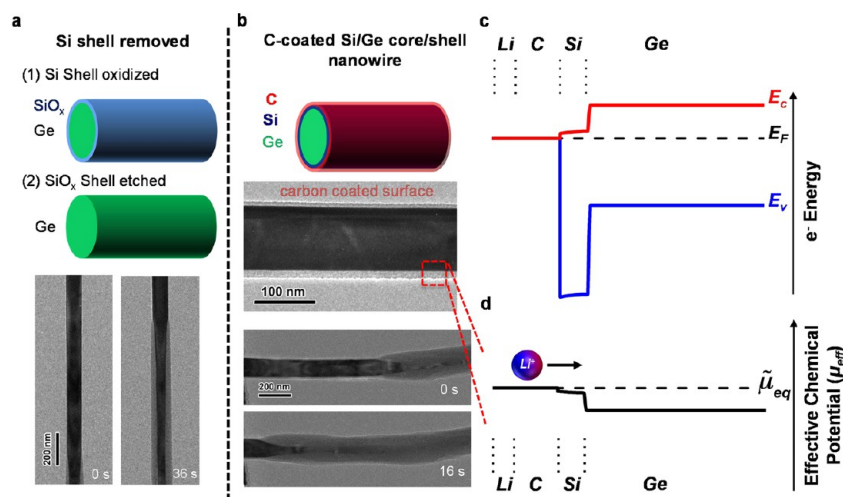
Figure 5. Control experiments under different scenarios to verify the proposed mechanism and their chemical potential profile. (a) Core−shell lithiation behavior of the Ge/Si core/shell nanowire after the Si shell was removed by a two-step striping method, using Si oxidization and followed by HF etching. (b) Core−shell lithiation behavior of carbon-coated Ge/Si core/shell nanowire. (c) Energy band-edge profile of the structure in (b) showing a large positive electron Schottky barrier between carbon and the Si shell. (d) The effective chemical potential for Li ions for the carbon-coated Ge/Si core/shell nanowire showing a potential well at the carbon/Si interface that leads to accelerated lithiation in carbon-coated nanowires.

In a Ge/Si core/shell nanowire, Li ions can diffuse through and react at either the cylindrical surface Si shell or the flat Ge surface in the core (left inset of Figure 4). Because μ_{eff} at the Ge interface is lower than that at the Si interface, the lithiation reaction in the Ge core proceeds at a much faster rate than at the surface and completely dominates the lithiation process. This is in contrast to the pure Ge nanowire case where the Li ions that quickly encapsulate the nanowire surface prior to triggering the lithiation process with external bias, experiences an already small chemical potential barrier at the surface and results in surface lithiation, leading to the observed tapered reaction front (right inset of Figure 4). We also note impurity diffusion coefficients in tensile-strained Si layers grown on relaxed SiGe layers were found to be smaller than that in relaxed Si.[50] The tensile strain in our Si shells were found to have as much as 3%,[51] which may contribute to the slower lithiation rates at the Si surface in the Ge/Si core/shell nanowires. A complete model for the chemical potential barriers for Li ion diffusion should take into account the influence of strain on energy band-edges and offsets through well-known deformation potentials.[52] Our experimental findings and qualitative analysis urges more detailed theoretical models that can fully capture the various components of chemical potential barriers in heterostructured nanowires.

From the above experiments and chemical potential analysis on pure Ge and Ge/Si core/shell nanowires, it is clear that the chemical potential barrier provided by the Si shell is very important to the control of lithiation behavior. To further validate this hypothesis, several control experiments were conducted. First, the surface Si shell was converted to SiO_x using an oxygen plasma treatment. The lithiation behavior of the Ge/SiO_x core/shell nanowire was changed from axial lithiation back to the core−shell lithiation similar to that observed for a pure Ge nanowire, as shown in Supporting Information Figure S6. Samples for which the surface SiO_x layer was removed by HF etch also exhibited a similar core−shell lithiation behavior (Figure 5a and Supporting Information Figure S7 and Movie S3).

Carbon coatings have been shown to improve the rate performance of lithium-ion batteries, by increasing the

electrodes' conductivity and accelerating the lithiation rates.[53] For radio frequency (RF) magnetron-sputtered carbon films on n-type Si, the tetrahedral amorphous carbon−silicon interface was characterized with a small positive electron barrier height, $0.01 \leq q\varphi_{Bn} \leq 0.1$ eV in the temperature range of 300−80 K.[54] Figure 5c shows the energy band-edge profile across 20 nm from the surface of a Ge/Si core/shell coated with C and Li. From eq 1, the small positive electron barrier height indicates a negative effective chemical potential for Li ions at the C/semiconductor interface as shown in Figure 5d, or in effect, a chemical potential well for Li ions, which is therefore expected to accelerate the lithiation reaction at the surface of the nanowire. Indeed, when carbon layers of 7−10 nm thick were coated on the Ge/Si core/shell nanowires, core−shell lithiation was observed in our experiments (Figure 5b and Supporting Information Movie S4).

One might suppose that the axial lithiation behavior can be attributed to the 400 times smaller diffusivity of Li in Si than in Ge.[55,56] However, the diffusivity difference cannot independently explain our observations without the influence of bandgap engineering effects discussed above. We first note that in our experiments, we found that the surface diffusion of Li ion on the surface of the Ge/Si core/shell nanowire is very fast, resulting a Li_2O layer on the surface due to the residual oxygen in the TEM column (Figure 1i), which can provide the medium for Li ion diffusion inward to initiate radial lithiation such as the case for the pure Ge nanowire. Utilizing the Nernst−Planck relationship,[57] one can estimate based on pure diffusivity differences a ratio for the lithiation lengths, L_{Si} in Si and L_{Ge} in Ge, to be $L_{Si}/L_{Ge} \cong D_{Si}\xi_{Si}/D_{Ge}\xi_{Ge} = 1/400$ for $\xi_{Si} = \xi_{Ge}$ is the electric field. Considering the surface Si layer is only about 1 nm, the radial lithiation should be triggered after axial lithiation of a length of about 400 nm along the nanowire when the surface Si layer should be fully lithiated. However, only axial lithiation persists during the whole lithiation process, indicating that the Li ion cannot diffuse inward from the surface, which strongly supports that the interface and interfacial chemical potential barriers manifested by bandgap engineering effects play an important role in the axial lithiation behavior observed in our studies.

The above set of experiments and discussions establishes that the axial lithiation in radially heterostructured nanowires is of a chemical potential origin. Increased Si shell thicknesses of 3 and 5 nm were employed to further substantiate the Si shell effect. Axial lithiation and elongation were observed in both samples (Supporting Information Figures S8 and S9). Further increase of the thickness of Si shell thickness beyond 5 nm would introduce surface roughening and grain boundary/twin formation in the Si shell[51] and was therefore avoided. Nevertheless, an ultrathin layer of Si as small as 1 nm is dramatically effective in controlling the Li ion transport through and reaction with the bulk Ge nanowire, an effect almost impossible to achieve with a purely mechanical confining layer.[22] It is important to note here that since the lithiation is dominated by the Ge nanowire core, the lithiated Ge nanowire core and Si shell are expected to lithiate disproportionally. Supporting Information Figures S8 and S9 show that island-like lithiated Si segments appear on the surface of the lithiated Ge nanowire, which is likely due to cracking of the Si shell after the lithiation of the Ge core and the later lithiation of the Si shell to form the island-like structures on the surface of the lithiated Ge core.

The control of volume expansion is extremely difficult for high-energy anode materials such as Si, Ge, Sn and their compounds, which may exhibit isotropic or orientation-dependent expansions up to 300% upon lithiation. Thus mechanical confinement has demonstrated limited success. Our experiments demonstrate an alternative strategy, that is, tailoring the electronic and interface properties of materials, which can be highly effective in defining the Li transport and electrode reactions with minimum added weight.

Conclusions. In summary, lithiation processes of individual pure Ge nanowires and Ge nanowires with various surface treatments were investigated by in situ transmission electron microscopy. Two different lithiation behaviors with sharp contrast, that is, core/shell lithiation in pure Ge nanowires versus axial lithiation in Ge/Si core/shell nanowires, were observed, which indicate two different Li ion transport mechanisms. The introduction of a Si/Ge heterojunction has significant impact on the Li ion transport and reaction. The presence of the Si shell slows down the lithiation reaction at the surface and forms a chemical potential barrier that blocks Li ion diffusion through the shell, resulting in the axial lithiation of the Ge/Si core/shell nanowires. This work is the first direct observation of the dramatic interfacial effect on ionic transport at the nanoscale and also the first demonstration that the lithiation behavior of a nanostructure can be controlled by interface and band gap engineering. Our work highlights the potential importance of materials design of lithium ion battery electrodes and proves a new and effective way to control the volume expansion of high-energy anode materials.

ASSOCIATED CONTENT

Ⓢ Supporting Information

Further details of experimental methods (materials synthesis, surface treatments, in situ TEM electrochemical lithiation setup and energy band-edge simulations), electron beam effect experiments, a set of control experiments, and movies. This material is available free of charge via the Internet at http://pubs.acs.org.

AUTHOR INFORMATION

Corresponding Authors
*E-mail: ynliu@sandia.gov.
*E-mail: sdayeh@ece.ucsd.edu.

Author Contributions
[⊥]Y.L. and X.H.L. contributed equally to this work.

Notes
The authors declare no competing financial interests.

ACKNOWLEDGMENTS

REFERENCES

(1) Tarascon, J. M.; Armand, M. *Nature* **2001**, *414* (6861), 359−367.
(2) Goodenough, J. B.; Kim, Y. *Chem. Mater.* **2009**, *22* (3), 587−603.
(3) Li, H.; Wang, Z.; Chen, L.; Huang, X. *Adv. Mater.* **2009**, *21* (45), 4593−4607.
(4) Larcher, D.; Beattie, S.; Morcrette, M.; Edstrom, K.; Jumas, J.-C.; Tarascon, J.-M. *J. Mater. Chem.* **2007**, *17* (36), 3759−3772.
(5) Park, C.-M.; Kim, J.-H.; Kim, H.; Sohn, H.-J. *Chem. Soc. Rev.* **2010**, *39* (8), 3115−3141.
(6) Besenhard, J. O.; Hess, M.; Komenda, P. *Solid State Ionics* **1990**, *40−41* (Part 2), 525−529.
(7) Ji, L.; Lin, Z.; Alcoutlabi, M.; Zhang, X. *Energy Environ. Sci.* **2011**, *4* (8), 2682−2699.
(8) Chan, C. K.; Peng, H.; Liu, G.; McIlwrath, K.; Zhang, X. F.; Huggins, R. A.; Cui, Y. *Nat. Nanotechnol.* **2008**, *3* (1), 31−35.
(9) Wu, H.; Chan, G.; Choi, J. W.; Ryu, I.; Yao, Y.; McDowell, M. T.; Lee, S. W.; Jackson, A.; Yang, Y.; Hu, L.; Cui, Y. *Nat. Nanotechnol.* **2012**, *7* (5), 310−315.
(10) Chan, C. K.; Zhang, X. F.; Cui, Y. *Nano Lett.* **2007**, *8* (1), 307−309.
(11) Lee, J. K.; Smith, K. B.; Hayner, C. M.; Kung, H. H. *Chem. Commun.* **2010**, *46* (12), 2025−2027.
(12) Hu, L.; Wu, H.; Hong, S. S.; Cui, L.; McDonough, J. R.; Bohy, S.; Cui, Y. *Chem. Commun.* **2011**, *47* (1), 367−369.
(13) Liu, X. H.; Huang, J. Y. *Energy Environ. Sci.* **2011**, *4* (10), 3844−3860.
(14) Liu, X. H.; Liu, Y.; Kushima, A.; Zhang, S.; Zhu, T.; Li, J.; Huang, J. Y. *Adv. Energy Mater.* **2012**, *2* (7), 722−741.
(15) Liu, X. H.; Zheng, H.; Zhong, L.; Huang, S.; Karki, K.; Zhang, L. Q.; Liu, Y.; Kushima, A.; Liang, W. T.; Wang, J. W.; Cho, J.-H.; Epstein, E.; Dayeh, S. A.; Picraux, S. T.; Zhu, T.; Li, J.; Sullivan, J. P.;

Cumings, J.; Wang, C.; Mao, S. X.; Ye, Z. Z.; Zhang, S.; Huang, J. Y. *Nano Lett.* **2011**, *11* (8), 3312−3318.

(16) Lee, S. W.; McDowell, M. T.; Choi, J. W.; Cui, Y. *Nano Lett.* **2011**, *11* (7), 3034−3039.

(17) Goldman, J. L.; Long, B. R.; Gewirth, A. A.; Nuzzo, R. G. *Adv. Funct. Mater.* **2011**, *21* (13), 2412−2422.

(18) Yang, H.; Huang, S.; Huang, X.; Fan, F.; Liang, W.; Liu, X. H.; Chen, L.-Q.; Huang, J. Y.; Li, J.; Zhu, T.; Zhang, S. *Nano Lett.* **2012**, *12* (4), 1953−1958.

(19) Liu, X. H.; Wang, J. W.; Huang, S.; Fan, F.; Huang, X.; Liu, Y.; Krylyuk, S.; Yoo, J.; Dayeh, S. A.; Davydov, A. V.; Mao, S. X.; Picraux, S. T.; Zhang, S.; Li, J.; Zhu, T.; Huang, J. Y. *Nat. Nanotechnol.* **2012**, *7* (11), 749−756.

(20) Liu, X. H.; Huang, S.; Picraux, S. T.; Li, J.; Zhu, T.; Huang, J. Y. *Nano Lett.* **2011**, *11* (9), 3991−3997.

(21) Chan, M. K. Y.; Long, B. R.; Gewirth, A. A.; Greeley, J. P. *J. Phys. Chem. Lett.* **2011**, *2* (24), 3092−3095.

(22) Zhang, L. Q.; Liu, X. H.; Liu, Y.; Huang, S.; Zhu, T.; Gui, L.; Mao, S. X.; Ye, Z. Z.; Wang, C. M.; Sullivan, J. P.; Huang, J. Y. *ACS Nano* **2011**, *5* (6), 4800−4809.

(23) Cho, J.-H.; Li, X.; Picraux, S. T. *J. Power Sources* **2012**, *205* (0), 467−473.

(24) Maier, J. *Nat. Mater.* **2005**, *4* (11), 805−815.

(25) Maier, J. *Solid State Ionics* **2004**, *175* (1−4), 7−12.

(26) Tuller, H. L. *Solid State Ionics* **2000**, *131* (1−2), 143−157.

(27) Beaulieu, L. Y.; Larcher, D.; Dunlap, R. A.; Dahn, J. R. *J. Electrochem. Soc.* **2000**, *147* (9), 3206−3212.

(28) Sata, N.; Eberman, K.; Eberl, K.; Maier, J. *Nature* **2000**, *408* (6815), 946−949.

(29) Xiang, J.; Lu, W.; Hu, Y.; Wu, Y.; Yan, H.; Lieber, C. M. *Nature* **2006**, *441* (7092), 489−493.

(30) Lu, W.; Xiang, J.; Timko, B. P.; Wu, Y.; Lieber, C. M. *Proc. Natl. Acad. Sci. U.S.A.* **2005**, *102* (29), 10046−10051.

(31) Peng, J. W.; Singh, N.; Lo, G. Q.; Kwong, D. L.; Lee, S. J. In *CMOS compatible Ge/Si core/shell nanowire gate-all-around pMOSFET integrated with HfO₂/TaN gate stack*, Electron Devices Meeting (IEDM), 2009 IEEE International, Dec. 7−9 2009; pp 1−4.

(32) Kroemer, H. *Proc. IEEE* **1963**, *51* (12), 1782−1783.

(33) Pei, Y.; Wang, H.; Snyder, G. J. *Adv. Mater.* **2012**, *24* (46), 6125−6135.

(34) Yin, W.-J.; Tang, H.; Wei, S.-H.; Al-Jassim, M. M.; Turner, J.; Yan, Y. *Phys. Rev. B* **2010**, *82* (4), 045106.

(35) Karki, K.; Epstein, E.; Cho, J.-H.; Jia, Z.; Li, T.; Picraux, S. T.; Wang, C.; Cumings, J. *Nano Lett.* **2012**, *12* (3), 1392−1397.

(36) Ghassemi, H.; Au, M.; Chen, N.; Heiden, P. A.; Yassar, R. S. *ACS Nano* **2011**, *5* (10), 7805−7811.

(37) McDowell, M. T.; Ryu, I.; Lee, S. W.; Wang, C.; Nix, W. D.; Cui, Y. *Adv. Mater.* **2012**, *24* (45), 6034−6041.

(38) Sun, C.-F.; Karki, K.; Jia, Z.; Liao, H.; Zhang, Y.; Li, T.; Qi, Y.; Cumings, J.; Rubloff, G. W.; Wang, Y. *ACS Nano* **2013**, *7* (3), 2717−2724.

(39) Gu, M.; Li, Y.; Li, X.; Hu, S.; Zhang, X.; Xu, W.; Thevuthasan, S.; Baer, D. R.; Zhang, J.-G.; Liu, J.; Wang, C. *ACS Nano* **2012**, *6* (9), 8439−8447.

(40) McDowell, M. T.; Woo Lee, S.; Wang, C.; Cui, Y. *Nano Energy* **2012**, *1* (3), 401−410.

(41) Wang, C.-M.; Li, X.; Wang, Z.; Xu, W.; Liu, J.; Gao, F.; Kovarik, L.; Zhang, J.-G.; Howe, J.; Burton, D. J.; Liu, Z.; Xiao, X.; Thevuthasan, S.; Baer, D. R. *Nano Lett.* **2012**, *12* (3), 1624−1632.

(42) Wang, X.; Tang, D.-M.; Li, H.; Yi, W.; Zhai, T.; Bando, Y.; Golberg, D. *Chem. Commun.* **2012**, *48* (40), 4812−4814.

(43) Wang, F.; Yu, H.-C.; Chen, M.-H.; Wu, L.; Pereira, N.; Thornton, K.; Van der Ven, A.; Zhu, Y.; Amatucci, G. G.; Graetz, J. *Nat. Commun.* **2012**, *3*, 1201.

(44) Dayeh, S. A.; Wang, J.; Li, N.; Huang, J. Y.; Gin, A. V.; Picraux, S. T. *Nano Lett.* **2011**, *11* (10), 4200−4206.

(45) Tersoff, J. *Phys. Rev. Lett.* **1990**, *65* (7), 887−890.

(46) Sze, S. M.; Ng, K. K. *Physics of Semiconductor Devices*, 3rd ed.; Wiley-Interscience: New York, 2007.

(47) Li as the shallow donors in Ge. http://www.ioffe.ru/SVA/NSM/Semicond/Ge/bandstr.html.

(48) Metal-Semiconductor Ohmic and Schottky Contacts. http://www.cleanroom.byu.edu/ohmic-schottky.phtml.

(49) Fuller, C. S.; Ditzenberger, J. A. *Phys. Rev.* **1953**, *91* (1), 193−193.

(50) Kringhøj, P.; Larsen, A. N.; Shirayev, S. Y. *Phys. Rev. Lett.* **1996**, *76* (18), 3372−3375.

(51) Dayeh, S. A.; Tang, W.; Boioli, F.; Kavanagh, K. L.; Zheng, H.; Wang, J.; Mack, N. H.; Swadener, G.; Huang, J. Y.; Miglio, L.; Tu, K.-N.; Picraux, S. T. *Nano Lett.* **2013**, *13* (5), 1869−1876.

(52) Fischetti, M. V.; Laux, S. E. *J. Appl. Phys.* **1996**, *80* (4), 2234−2252.

(53) Liu, X. H.; Zhang, L. Q.; Zhong, L.; Liu, Y.; Zheng, H.; Wang, J. W.; Cho, J.-H.; Dayeh, S. A.; Picraux, S. T.; Sullivan, J. P.; Mao, S. X.; Ye, Z. Z.; Huang, J. Y. *Nano Lett.* **2011**, *11* (6), 2251−2258.

(54) Hastas, N. A.; Dimitriadis, C. A.; Logothetidis, S.; Angelis, C. T.; Konofaos, N.; Evangelou, E. K. *Semicond. Sci. Technol.* **2001**, *16*, 474.

(55) Graetz, J.; Ahn, C. C.; Yazami, R.; Fultz, B. *J. Electrochem. Soc.* **2004**, *151* (5), A698−A702.

(56) Fuller, C. S.; Severiens, J. C. *Phys. Rev.* **1954**, *96* (1), 21−24.

(57) Park, M.; Zhang, X.; Chung, M.; Less, G. B.; Sastry, A. M. *J. Power Sources* **2010**, *195* (24), 7904−7929.